Aerodynamic analysis involving moving parts with XFlow

This report presents some of the possibilities of XFlow 2011, specifically those related to the aerodynamic analysis of moving parts. Using traditional Computational Fluid Dynamics (CFD) software, this kind of problems require time consuming remeshing processes, which often lead to errors or divergence of the simulation. Due to the particle-based fully Lagrangian approach of XFlow, moving parts such as a vehicle with suspension system or the forced rotation of the wheels can be easily handled, namely the only parameters required as input are the physical and mechanical properties of the objects. Furthermore, full vehicle models can be directly used in the simulation, and thus the complexity of the surfaces is not a limiting factor.

1: Introduction

The development of vehicle aerodynamics based on a combination of virtual and physical methods has become an integral part of the design process. When aerodynamic forces are calculated, the change of ride height due to lift forces acting on the vehicle is often neglected. This approach might be applicable for "standard cars", but may lead to misleading results for sports and race cars, where large downforce values change ride heights substantially (Drage and Riedler, 2009). Using the software presented here, it is possible to simulate the vehicle full (6 DOFs) movement according to the aerodynamic forces.

2: Numerical Methodology

In the literature there are several particle-based numerical approaches to solve the computational fluid dynamics. They can be classified in three main categories: Algorithms modelling the behaviour of the fluid at microscopic scale (e.g. Direct Simulation Montecarlo); algorithms which solve the equations at a macroscopic level, such as Smoothed Particle Hydrodynamics (SPH) or Vortex Particle Method (VPM); and finally, methods based on a mesoscopic framework, such as the Lattice Gas Automata (LGA) and Lattice Boltzmann Method (LBM).

The algorithms that work at molecular level have a limited application, and they are used mainly in theoretical analysis. The methods that solve macroscopic continuum equations are employed most frequently, but they also present several problems. SPH-like schemes are computationally expensive and in their less sophisticated implementations show lack of consistency and have problems imposing accurate boundary conditions. VPM schemes have also a high computational cost and besides, they require additional solvers (e.g. schemes based on boundary element method) to solve the pressure field, since they only model the rotational part of the flow.

Finally, LGA and LBM schemes have been intensively studied in the last years being their affinity to the computational calculation their main advantage. Their main disadvantage is the complexity to analyze theoretically the emergent behaviour of the system from the laws imposed at mesoscopic scale. XFlow's approach to the fluid

physics takes the main ideas behind these algorithms and extends them to overcome most of the limitations present on these schemes.

2.1: Lattice Gas Automata

LGA schemes are simple models that allow solving the behaviour of gases. The main idea is that the particles move discretely in a *d*-dimensional lattice in one of the predetermined direction at discrete times $t = 0, 1, 2,...$ and with velocity c_i, $i = 0, ...,b$, also predetermined.

The simplest model is the HPP, introduced by Hardy, Pomeau and de Pazzis, in which the particles move in a two-dimensional square grid and in four directions. The state of an element of the lattice at instant *t* is given by the occupation number $n_i\ (r; t)$, with $i = 0, ..., b$, being $n_i = 1$ presence and $n_i = 0$ absence of particles moving in direction *i*.

The equation that governs the evolution of the system is as follows:

$$n_i\left(r + c_i\Delta t, t + \Delta t\right) = n_i(r,t) + \Omega_i(n_1,...,n_b)\Big)$$

where Ω_i is the collision operator, which for each previous state $(n_1,...,n_b)$ computes a post-collision state $(n_1^C,...., n_b^C)$ conserving the mass, linear momentum and energy, *r* is a position in the lattice and c_i a velocity.

From a statistical point of view, a system is constituted by a large number of elements which are macroscopically equivalent to the system investigated. The macroscopic density and linear momentum are:

$$\rho = \frac{1}{b}\sum_{i=1}^{b} n_i \qquad\qquad \rho v = \frac{1}{b}\sum_{i=1}^{b} n_i c_i$$

2.2: Boltzmann's transport equation

Boltzmann's transport equation is defined as follows:

$$f_i(r + c_i\Delta t, t + \Delta t) = f_i(r,t) + \Omega_i^B(f_1,..., f_b)$$

where f_i is the distribution function in the direction *i* and Ω_i^B the collision operator.

From this equation and by means of the Chapman-Enskog expansion, the compressible Navier-Stokes equations can be recovered.

The main advantage of these methods is their great affinity with computers. They are easily programmed and very efficient. Some schemes have isotropy problems (do not satisfy Galilean invariance) and produce very noisy results. The main contribution of LGA schemes is that they were precursor of the Lattice Boltzmann method.

2.3: Lattice Boltzmann method

The origins of the Lattice Boltzmann Method (LBM) (Chen, Chen and Matthaeus, 1992; Higuera and Jimenez, 1989; McNamara and Zanetti, 1988) lie in the LGA schemes. While the LGA schemes use discrete numbers to represent the state of the

molecules, the LBM method makes use of statistical distribution functions with real variables, preserving by construction the conservation of mass, linear momentum and energy. It can be shown that if the collision operator is simplified under the Bhatnagar-Gross-Krook (BGK) approximation, the resulting scheme reproduces the hydrodynamic regime also for low Mach numbers. This operator is defined as follows:

$$\Omega_i^{BGK} = \frac{1}{\tau}\left(f_i^{eq} - f_i\right)$$

where f^i_{eq} is the local equilibrium function and τ is the relaxation characteristic time, which is related to the macroscopic viscosity in the following way:

$$\nu = c_s^2\left(\tau - \frac{1}{2}\right)$$

with c_s the speed of sound. For a positive viscosity, the relaxation time must be greater than 0.5. The most interesting aspect is that these schemes are able to model a wide range of viscosities in an efficient way even using explicit formulations.

2.4: Turbulence modelling

The approach used for turbulence modelling is the Large Eddy Simulation (LES). These schemes solve the turbulence in a local way, modelling only the smallest scales, and are closer to the physics. The turbulence at smallest scales has been extensively studied and its behaviour can be reproduced without using arbitrary parameters.

The LES scheme adopted by default by XFlow is the Wall-Adapting Local Eddy viscosity (WALE) (Nicoud and Ducros, 1999), which has good properties both near and far of the wall and in laminar and turbulent flows.

2.5: Treatment of moving geometries

The treatment of moving boundary conditions is straightforward and similar to the handling of fixed boundaries. In basic LBM implementations the wall boundary conditions for straight boundaries are typically implemented following a simple bounce-back rule for the no-slip boundary condition and a bounce-forward rule for the free-slip. In XFlow the statistical distribution functions f_i coming from the boundaries are reconstructed taking into account the wall distance, the velocity and the surface properties. The set of statistical distribution functions to be reconstructed is recomputed each time-step based on the updated position of the moving boundaries. A reference distance to the wall, velocity, surface orientation and curvatures are taken into account in order to solve the wall boundary condition.

As the physics are not implemented using surface elements XFlow relaxes the requirements imposed to the geometries and is tolerant to crossing or complex surfaces. Finally, a unified non-equilibrium law of the wall model takes into account for the under-resolved scales at the boundary layer.

3: Numerical results

In this section we will show the capabilities of XFlow for simulating the dynamic vehicle response to changing flow conditions in two cases: a simplified reference model and a real race car. In the first case we will compare the behaviour of the suspension system in conditions of regular aerodynamic forces (vertical displacement and pitching) and gusty side wind (with rolling as additional DOF). For the real race car we will include the effect of the rotating wheels and compare the suspension behaviour at different ride velocities. Finally, we also simulate the maneuver of a car overtaking a truck and measure the forces experienced by both vehicles.

3.1: Simplified reference car

The model chosen is the well known "Aerodynamisches Studienmodel" (ASMO). It comprises a square-back rear, smooth surfaces, boat tailing, underbody diffuser and no pressure induced boundary layer separation (Perzon and Davidson, 2000). The geometry has a well defined separation line and is characterized by a low drag shape. For this model, experimental data from Daimler Benz and the Volvo model scale wind tunnel are available.

CFD validations using the ASMO have already been published by several authors. Perzon and Davidson (2000) showed that using transient CFD simulations, surface pressure values can be computed fairly accurate. The overall drag coefficient however, is not predicted satisfactorily.

The present simulations are performed using a wind tunnel of dimensions 9 x 1.5 x 3m (which corresponds to a blockage ratio of 1.38%) and Reynolds number Re=2.7x10^6 (taking the length of the vehicle as reference). Particle resolution in the far field is 0.1m, while in the wake and on the model surface, scales up to 2.5mm are resolved. Dynamic wake refinement is applied, so the particle resolution is automatically adopted in regions with high turbulence, while less turbulent regions are treated with fewer particles. The initial number of particles is 1 million, while at final time t=0.25 the number of particles achieves 20 million.

Figure 1: Snapshot of isosurfaces of vorticity

Typically, drag stabilizes in a characteristic time in the order of the time required for the flow to travel along the vehicle length. In 0.1 seconds, the flow has travelled more than six times the whole body. The time averaged drag coefficient between 0.05 and 0.1 seconds of physical simulation is c_d = 0.151, which is in good agreement with the values measured in the experiments, shown in Table 1. RANS turbulence models tend to overestimate the drag.

Simulation XFlow	0.151
Experiments Volvo	0.158
Experiments Daimler Benz	0.153

Table 1: drag coefficient of the ASMO

Figure 2 shows validation results of surface pressure measurements, which have been performed both in the Volvo and the Daimler Benz wind tunnel. Data is available in the symmetry plane and is shown for roof, underbody, front and base region of the vehicle. It can be seen, that the comparison with the measurements is good, although some deviations can be observed. Especially the base pressure is slightly underpredicted, and shows some unphysical peak at the transition from roof to base. The proper level of the base pressure is not known exactly, as there is a large difference between the two experiments.

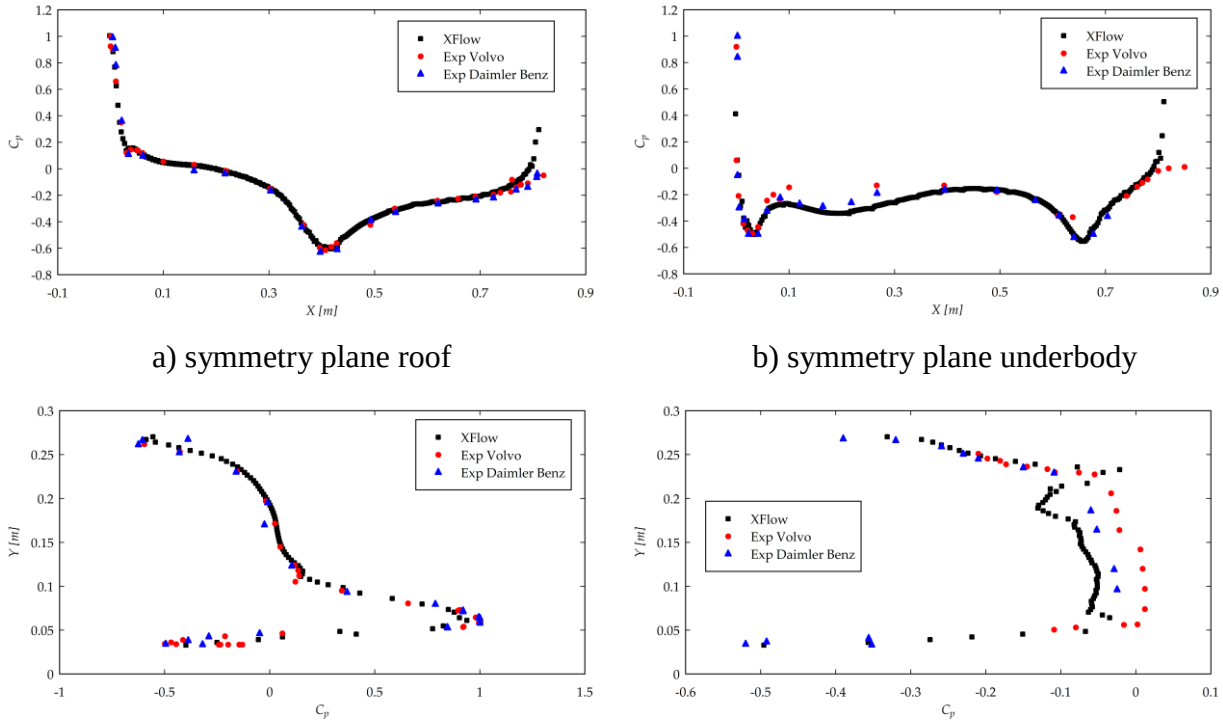

a) symmetry plane roof

b) symmetry plane underbody

c) symmetry plane front region

d) symmetry plane base

Figure 2: Comparison of surface pressure measurements with the simulation (Drage et al, 2010).

Next we show the results of the ASMO calculation when the vehicle position with respect to the ground is modified due to aerodynamic forces. Studies to analyze vehicle response to turbulence and side wind, or the effect of pitching and rolling motion have already been performed and published by several authors; see for example Schröck, Widdecke and Wiedemann (2009) and Tsubokura et al (2009).

For the analysis of the ASMO with pitching and vertical motion, the wheels have been separated from the main body and a wheel space has been created to allow the displacement of the main body. It is assumed that the vehicle is a rigid body of mass *m* and moment of inertia I_z with a suspension that will be modelled as a two-degree-of-freedom (DOF) system. The DOFs are: the bounce displacement about the body's centre of gravity (*y*, in meters) and the pitching angle (rotation with respect to the z-axis, α, in radians), see Figure 3. *k* and *c* are the equivalent spring stiffness and damping of the suspension respectively. The centre of gravity (CoG) has been defined slightly lower than the location of the geometrical centre to make it more realistic.

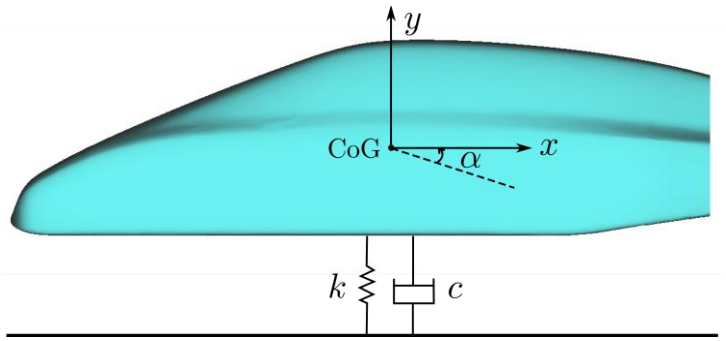

Figure 3: Schematic of the ASMO case with spring and damping element

The equations for the external force F_y and external moment M_z read:

$$F_y = m\,\ddot{y} = -c_1\,\dot{y} - k_1 y$$

$$M_z = I_z\,\ddot{\alpha} = -c_2\,\dot{\alpha} - k_2\alpha$$

and the values taken in the simulation are the following:

m	1	kg
I_z	0.009	Kg m^2
k_1	750	N m^{-1}
c_1	100	N s m^{-1}
k_2	25	N m^{-1}
c_2	5	N s m^{-1}

Table 2: Physical properties for the ASMO suspension system simulation

Figure 4 shows snapshots of velocity in the symmetry plane for different simulation times. It can be seen how the vehicle changes its vertical position due to aerodynamic forces. Specially in the underbody and diffusor region, the modified vehicle position changes the flow considerably.

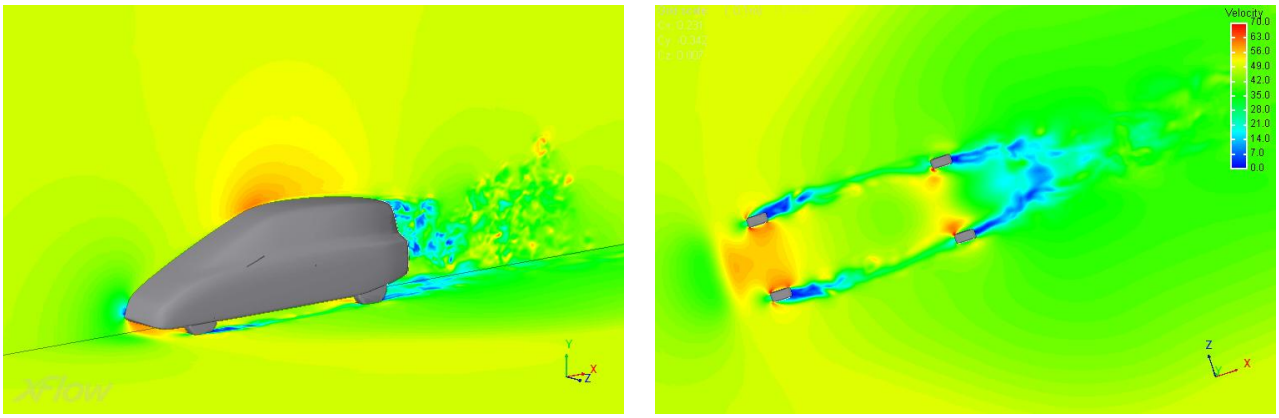

a) t = 0.2 s

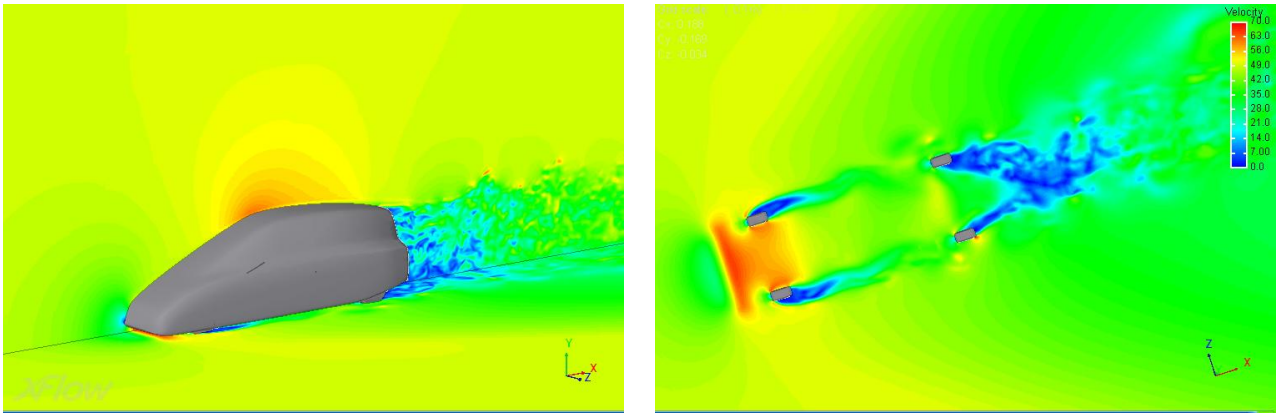

b) t= 0.25 s

Figure 4: Instantaneous velocity field at symmetry plane and ground plane.

In the case including rolling, the stiffness and damping coefficients for the rotational spring in x-direction (k_3 and c_3) are scaled by a factor of transversal distance/longitudinal distance between wheels = 0.4, so that k_3 = 10 N m^{-1} and c_3=2 N s m^{-1}. A side wind in z-direction of 50 km/h (13.88 m/s) was applied for the simulation. Because in the virtual wind tunnel domain type the boundary conditions in the z-direction are periodic, the lateral wind has been modelled as a variable external acceleration law; see Figure 5a.

Figures 5b and 5c compare the vertical displacement and pitching angle for the cases without and with side wind. We can observe that the vehicle position is automatically adapted to reach equilibrium. The presence of lateral forces cause a smaller displacement and slightly smaller pitching angles. The rolling (Figure 5d) is mainly caused by the gust. The changing flow conditions and the motion of the car body lead to an increase of the drag and side force coefficients (Figure 6).

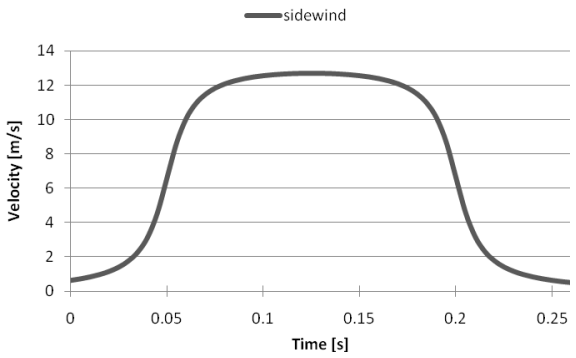

a) Side wind velocity (in m/s)

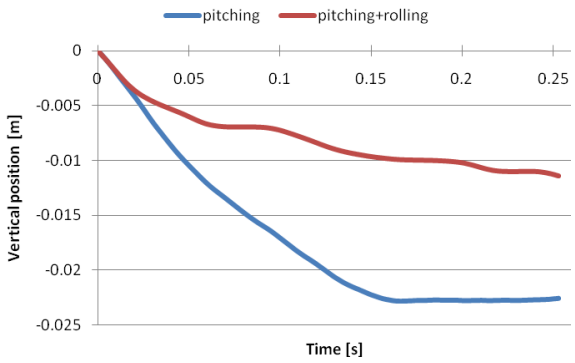

b) Vertical displacement at CoG (in meters)

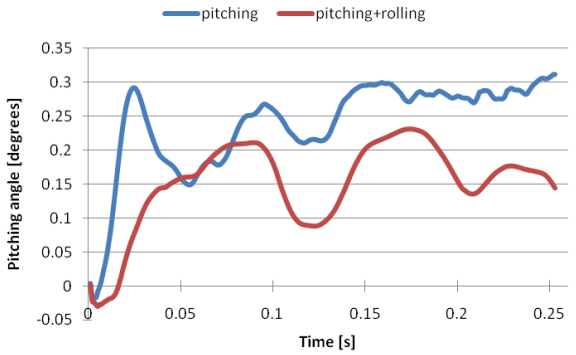

b) Pitching angle (in degrees)

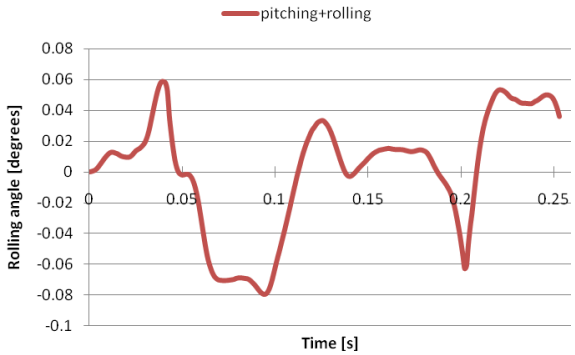

d) Rolling angle (in degrees)

Figure 5: Side wind velocity and comparison of vertical displacement, pitching and rolling angle

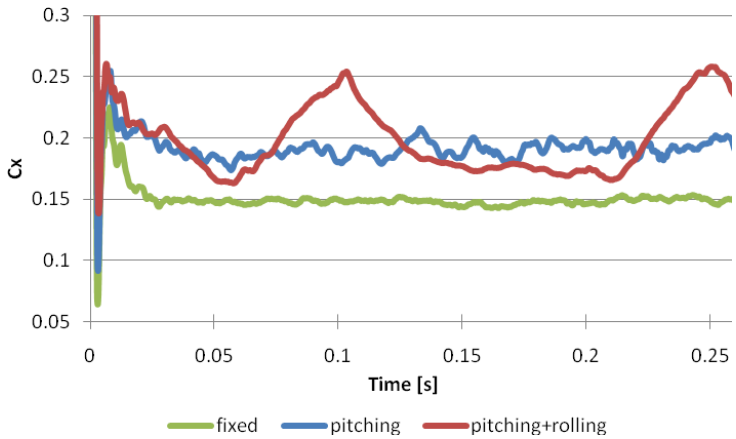

a) Drag coefficient

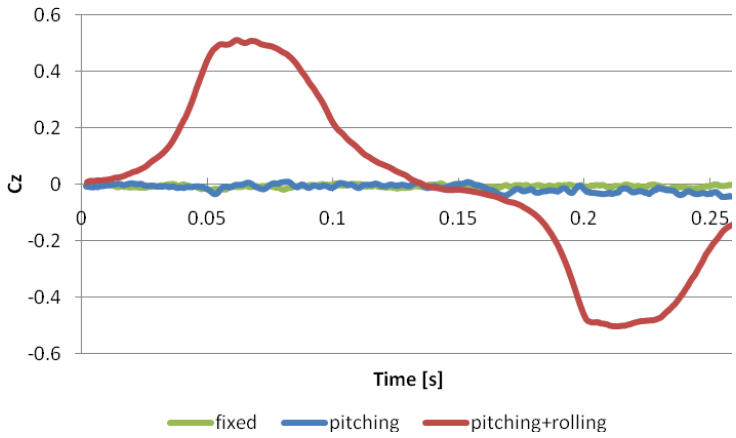

b) Side force coefficient

Figure 6: Comparison of drag and side force coefficients

3.2: Race car

The aerodynamics of race cars is highly dependent on ride height. Ride height again depends on aerodynamic forces, which in turn depend on vehicle setup and driving velocity. In this section we analyze the aerodynamics of the KTM XBow (see Figure 7) and compare the suspension behaviour at velocities 140 km/h and 200 km/h.

In the simulations 2 DOFs are enabled (vertical displacement and pitching), the weight of the vehicle and the spring forces in front and rear axles are set using the values provided by the manufacturer, and the wheels are modelled as real rotating parts. A resolution of 2 cm has been used close to the vehicle and in the wake. The initial ride height is approximately the equilibrium height at 140km/h.

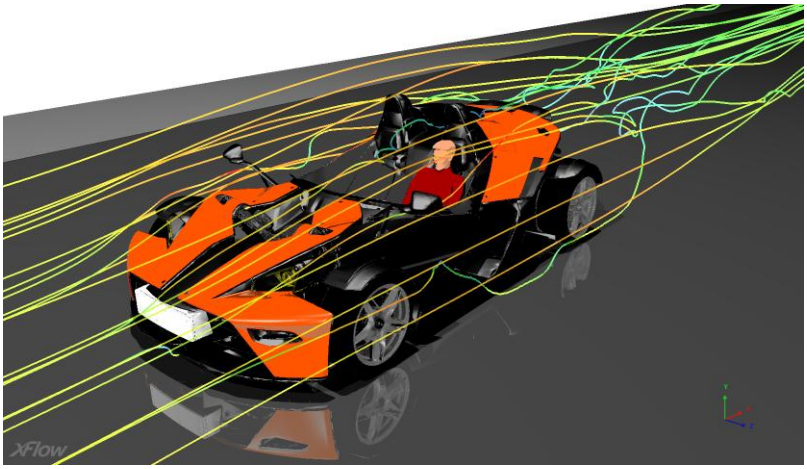

Figure 7: KTM XBow race car

The results are shown in Figure 8. As expected, the larger downforces at 200km/h cause larger vertical displacements and pitching angles.

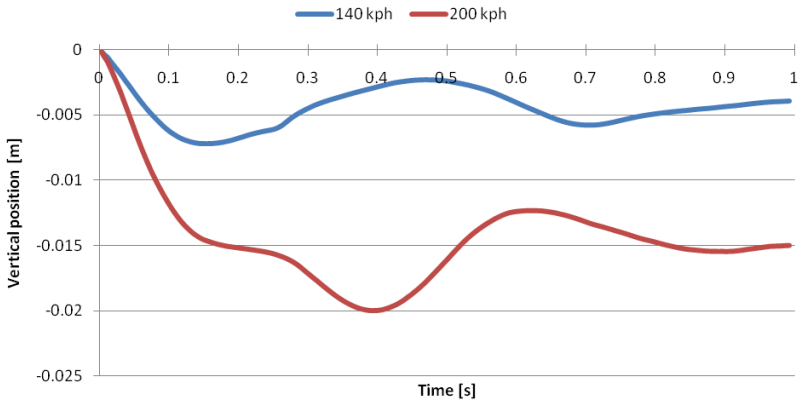

a) Vertical displacement at CoG (in meters)

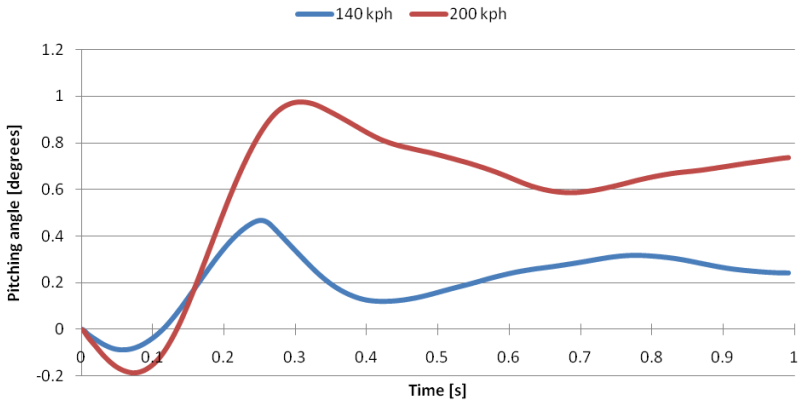

b) Pitching angle (in degrees)

Figure 8: Vertical displacement and pitching angle for the KTM XBow at 140 and 200 km/h

3.3: Overtaking maneuver

The last example is a proof of concept of an overtaking maneuver under side wind conditions; see Figure 9. The car follows a forced motion that describes the overtaking of a truck. The inlet flow velocity is of 30 m/s in x-direction and the lateral wind velocity of 20 m/s in z-direction.

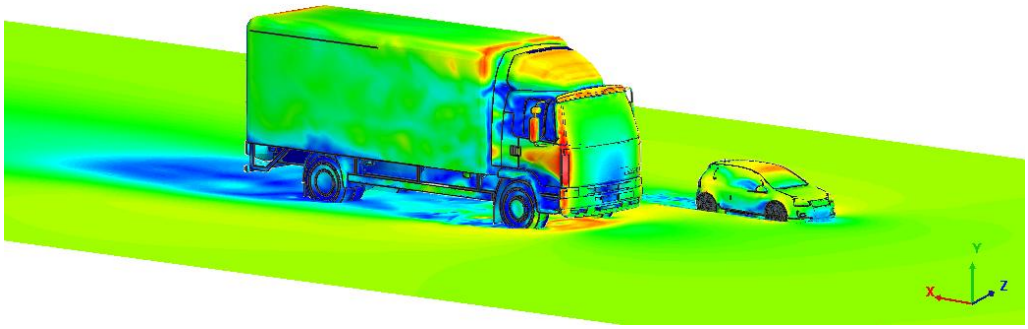

Figure 9: Car overtaking a slower truck

The simulation allows to monitor the evolution of the aerodynamic coefficients during the maneuver, as shown in Figure 10. For t<3 s the car is inside the wake of the truck and this causes its lateral wind force coefficient c_z to progressively decrease. From there on, c_z increases (due to the flow that passes under the truck) until reaching a maximum when the car overtakes the truck and is fully exposed to the wind. The car experiences a low drag while the car is within the wake of the truck and stabilizes at a reasonable value once the maneuver has finished. Forces on the truck remain quite uniform during the whole maneuver.

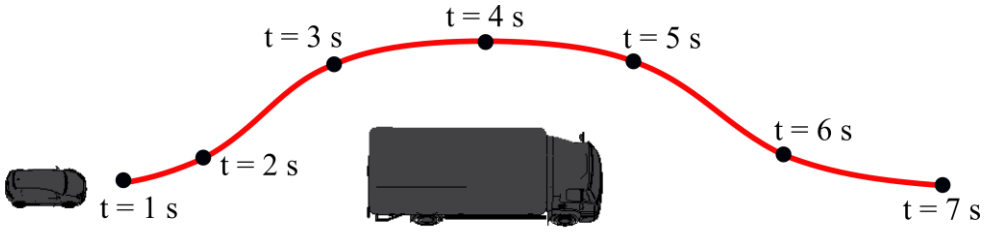

a) Trajectory of the car

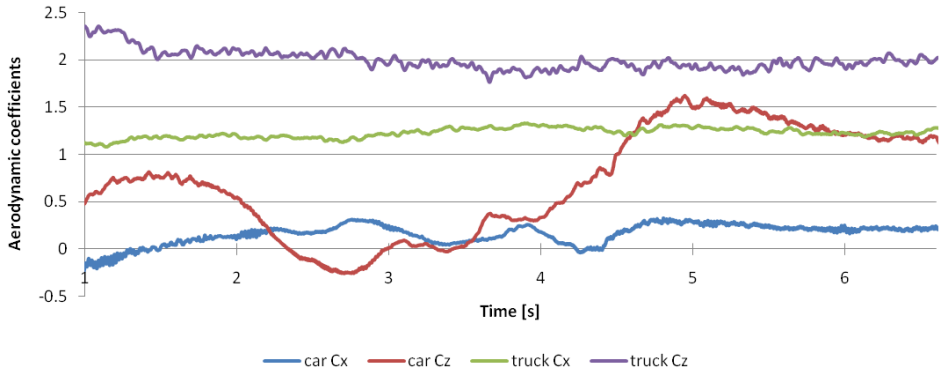

b) Aerodynamic coefficients of car and truck

Figure 10: Evolution of aerodynamic coefficients during overtaking

REFERENCES

Chen, H., Chen, S., and Matthaeus, W. (1992) "Recovery of the Navier-Stokes equations using a lattice-gas Boltzmann method", *Physical Review A*, vol. 45, pp. 5339.

Drage, P., and Riedler, S. (2009) "On the Aerodynamic Development of a Light Weight Sports Car by Means of CFD", *7th FKFS Conference*, Stuttgart.

Drage, P., Kussmann, C., Holman, D.M. and Mier-Torrecilla, M. (2010) "Simulation of Unsteady Aerodynamics using a Mesh-less Particle Approach", *8th MIRA International Vehicle Aerodynamics Conference*, pp. 446-456.

Higuera, F.J., and Jimenez, J.(1989) "Boltzmann approach to lattice gas simulations", *Europhysics Letters*, vol. 9, pp. 663-668.

McNamara, G., and Zanetti, G., (1988) "Use of the Boltzmann equation to simulate lattice-gas automata", *Physical Review Letters*, vol. 61, pp. 2332-2335.

Nicoud F. and Ducros F. (1999) "Subgrid-scale stress modeling based on the square of the velocity gradient tensor", *Flow, Turb. & Comb*., vol 62, pp. 183-200.

Perzon, S., and Davidson, L.(2000) "On Transient Modelling of the Flow Around Vehicles Using the Reynolds Equations", *ACFD 2000*, Beijing.

Schröck, D., Widdecke, N., Wiedemann, J.(2009) "Aerodynamic Response of a Vehicle Model to Turbulent Wind", *7th FKFS Conference*, Stuttgart.

Tsubokura, M., Nakashima, T., Kitoh, K., Sasaki, Y. (2009) "Development of Unsteady Aerodynamic Simulator Using Large-Eddy Simulation", *7th FKFS Conference*, Stuttgart.